Non-covalent strategies to functionalize polymeric nanoparticles with NGR peptides for targeting breast cancer

Claudia Conte[1], Giuseppe Longobardi[1], Antonio Barbieri[2], Giuseppe Palma[2], Antonio Luciano[2], Giovanni Dal Poggetto[3], Concetta Avitabile[4], Annalisa Pecoraro[1], Annapina Russo[1], Giulia Russo[1], Paola Laurienzo[3], Alessandra Romanelli[5], and Fabiana Quaglia[1,3]*

[1] Department of Pharmacy, University of Naples Federico II, Via D. Montesano 49, 80131, Naples, Italy

[2] Animal Facility Unit of Research Department of Istituto Nazionale Tumori "Fondazione Pascale", Via M. Semmola, 52 - 80131 Napoli (NA) Naples, Italy

[3] Institute for Polymers, Composites and Biomaterials, CNR, Via Campi Flegrei 34, 80078 Pozzuoli, Naples, Italy

[4] CNR-Institute of Crystallography, Via Vivaldi 43, 81100 Caserta

[5] University of Milan, Via Golgi, 19, 20133, Milan, Italy

KEYWORDS

Polymeric nanoparticles, NGR peptides, palmitoylation; breast cancer.

ABSTRACT

Surface functionalization of nanoparticles (NPs) with tumor-targeting peptides is an emerging approach with a huge potential to translate in the clinic and ameliorate the efficacy of nano-oncologicals. One major challenge is to find straightforward strategies for anchoring peptides on the surface of biodegradable NPs and ensuring their correct exposure and orientation to bind the target receptor. Here, we propose a non-covalent strategy to functionalize polyester aminic NPs based on the formation of either electrostatic or lipophilic interactions between NPs and the peptide modified with an anchoring moiety. We selected an iNGRt peptide containing a CendR motif (CRNGR) targeting neuropilin receptor 1 (NRP-1), which is upregulated in several cancers. iNGRt was linked with either a short poly(glutamic acid) chain (polyE) or a palmitoyl chain (Palm) and used to functionalize the surface of NPs made of a diamine poly(ε-caprolactone). iNGRt-PolyE was adsorbed on preformed cationic NPs through electrostatic interaction, whereas iNGRt-Palm was integrated into the forming NPs through hydrophobic bonds. In both cases, peptides were strongly associated with NPs of ~100 nm, low polydispersity indexes, and positive zeta potential values. NPs entered MDA-MB231 breast cancer cells overexpressing NRP-1 via receptor-mediated endocytosis and showed a different cell localization depending on the mode of peptide anchoring. When loaded with the lipophilic anticancer drug docetaxel (DTX), NPs functionalized with the iNGRt-Palm variant exerted a time- and dose-dependent cytotoxicity similar to DTX in MDA-MB231 but were less toxic than DTX toward control MR5 human fibroblasts, not expressing NRP-1. In a heterotopic mouse model of triple negative breast cancer, iNGRt-Palm NPs were tolerated better than free DTX and demonstrated superior anticancer activity and survival compared to both free DTX and NPs without peptide functionalization. We foresee that the functionalization strategy with palmitoylated peptides proposed here can be extended to other biodegradable NPs and peptide sequences designed for therapeutic or targeting purposes.

INTRODUCTION

The active targeting of nanomedicines is a promising strategy for improving clinical outcomes in cancer therapies but is still elusive in clinical practice (Pearce and O'Reilly, 2019). In particular, due to their safety profile, controlled release of bioactive cargo, tunable physicochemical properties, and surface features, polymeric NPs still represent an up-and-coming tool for pharmaceutical applications in several diseases, including cancer (Niza et al., 2021).

We have recently found that poly(ε-caprolactone) (PCL) suitably modified at the terminus with a primary amine gives stable positively-charged NPs with a tropism toward metastatic lung (Conte et al., 2019a; Esposito et al., 2018) and prolonged residence time in a simulated extracellular tumor matrix (Conte et al., 2019a). To expand the therapeutic potential of this class of NPs, it is crucial to find suitable surface functionalization strategies allowing selective tumor targeting. The design of an efficient actively-targeted nanoplatform requires an appropriate method to functionalize NP and a rational formulation strategy for precisely controlling targeting ligand display and, in parallel, size and surface charge. These properties impact the biological identity of NPs driving protein corona formation, blood circulation time, biodistribution, toxicity, and immunological response (Shi et al., 2017).

Among the wide panel of moieties available to functionalize the NP surface and recognize receptors typically over-expressed in tumors, functional targeting peptides have gained extensive attention (Seyyednia et al., 2021; Sun et al., 2018) since they can be identified through powerful technologies like phage-display, rationally designed by computational modelling and easily manufactured by solid-phase peptide synthesis (Fosgerau and Hoffmann, 2015).

Covalent and non-covalent strategies to functionalize biodegradable NPs with peptides specifically developed for tumor targeting have been recently reviewed (Gessner and Neundorf, 2020a; Ruoslahti, 2017; Seyyednia et al., 2021; Sun et al., 2018). Polymeric NPs displaying covalently linked peptides on the surface are either prepared from ad-hoc functionalized polymers (Brossard et al., 2021; Conte

et al., 2019b; Fan et al., 2018; Hoyos-Ceballos et al., 2020) or via post-modification after their preparation (Esfandyari-Manesh et al., 2020; Galindo et al., 2022; Li et al., 2011). This last strategy, highly suited for inorganic NPs (Aubin-Tam and Hamad-Schifferli, 2008; Delehanty et al., 2010; Gessner and Neundorf, 2020b), remains challenging for polymeric NPs in the perspective of scale-up. The orientation and density of the targeting molecule during the coupling reaction are poorly controlled, the release of drug cargo can occur, and the degradation of the polymer matrix can start (Gessner and Neundorf, 2020a). Furthermore, the purification from unreacted reagents and byproducts can be challenging for some materials and conjugation chemistry employed, finally impairing the safety of the final nanoconstruct. On the other hand, the non-covalent adsorption of peptides on the NP surface through electrostatic and/or hydrophobic interactions is, in principle, the most straightforward strategy for the functionalization of biodegradable NPs. While peptide adsorption is critically affected by the ionic strength and pH of the medium (Cai et al., 2017; Gessner and Neundorf, 2020b) anchoring of palmitoylated peptides onto preformed NPs through hydrophobic interaction seems promising (Paulino da Silva Filho et al., 2021).

As a target receptor, we focused on the neuropilin receptors-1 (NRP-1), a non-tyrosine kinase transmembrane receptor upregulated in several clinical disorders, including cancer. NRP-1 is recognized by peptides containing a CendR motif (RXXR) located at a C-terminus. In particular, NRP-1 mediates penetration into the tumour matrix due to its overexpression on both tumour endothelia and cancer cells (Jensen et al., 2015; Kadonosono et al., 2015), thus activating an endocytotic/exocytotic transport pathway, named CendR pathway (Ruoslahti, 2017; Teesalu et al., 2009). iNGR peptides contain a cryptic tissue penetration CendR motif, a vascular homing motif and a protease recognition site. iNGR initially binds the CD13 receptor on the endothelial cells and, upon proteolytic cleavage, forms a truncated peptide (iNGRt) that is recognized by NRP-1 and undergoes the CendR pathway (Ruoslahti, 2017). So far, different polymeric NPs have been surface-modified with iNGR and iNGRt peptides through covalent conjugation strategies (Sun et al., 2018). Despite

the efficacy of this system in deeply penetrating the tumour tissue, the conjugation efficiency of the peptide was only 60% (Kang et al., 2014), and the linkage implicated the use of organic solvents that could alter the safety of the system and its translational potential. Most of the reported peptide-directed polymeric nanomedicines do have a rather complex design requiring a multi-step reproducible fabrication process, which is one main drawback.

To facilitate clinical translation and reduce the complexity of the systems while maintaining the added targeting function, we explore here the suitability of two non-covalent strategies, adsorption or intercalation, to modify the surface of biodegradable NPs of diamine-PCL (daPCL) with NGR peptides. Three NGR peptides (iNGR, iNGRt, and NGR as control) were chemically modified with 5 units of glutamic acid (E5 sequence, PolyE) or a palmitoyl chain (Palm). The peptides derivatized with PolyE were adsorbed on preformed NPs through electrostatic interaction, whereas the Palm-variant was integrated into the polymeric matrix during NP formation. After a preliminary formulation study aimed at finding the optimized formulation conditions to obtain stable NGR-decorated NPs, their cytotoxicity and cell uptake/localization in triple-negative breast cancer cells (MDA-MB231) over-expressing NRP-1 (Kadonosono et al., 2015) were investigated. To provide a therapeutic proof-of-concept, NPs were loaded with Docetaxel (DTX), a conventional lipophilic anticancer drug with antimitotic activity, and their biological properties tested in vitro and in a heterotopic mouse model.

2 EXPERIMENTAL

2.1 Materials

Sodium Chloride, DAPI, poloxamer 188 (Pluronic F68) and methanol (MeOH) were from Sigma-Aldrich, Milan, Italy. 1,1′-Dioctadecyl-3,3,3′,3′-tetramethylindocarbocyanine perchlorate (DiI) and the Pierce™ Quantitative Colorimetric Peptide Assay kit were from Thermo Fisher Scientific, Monza, Italy. Dichloromethane (DCM) and acetone were from Honeywells, Monza, Italy. Docetaxel (DTX) was provided by Alpha Aesar. Potassium phosphate dibasic and potassium phosphate monobasic, sodium azide, potassium chloride, sodium phosphate dibasic, human serum albumin (HSA) and human plasma were used as received (Sigma-Aldrich, Italy). Dialysis membranes (MWCO 3500, regenerated cellulose) were used as received (Spectrapor, Italy). The amino-terminated H_2N-$PCL_{4.7K}$-NH_2 (daPCL) was synthesized and characterized as previously reported (Conte et al., 2019a).

2.2 Synthesis of the peptides

Peptides CendR (E5-Ahx- CRNGR and K(Palm)- Ahx- CRNGR), were synthesized on the Wang Chem matrix (Biotage) 0.39 mmol/g-resin. Controls (E5-Ahx-iNGR(cyclic), K(Palm)-Ahx-iNGR (cyclic), E5-Ahx-NGR(cyclic), K(Palm)-Ahx-NGR (cyclic)) were obtained by solid-phase synthesis following standard protocols (Bezzerri et al., 2014) on the Rink amide MBHA resin (0.54 mmol/g). Peptides were cleaved off the resin and deprotected by treatment of the resin with a solution of TFA/TIS/H_2O/EDT 95/2/1/2 v/v/v/v 90 min. TFA was concentrated, and peptides were precipitated in cold ethylic ether. Cyclic peptides were obtained by oxidation of the linear peptides following the protocol reported in (Bezzerri et al., 2014). Analysis of the crudes was performed by LC-MS on an LC-MS Agilent Technologies 6230 ESI-TOF using a Phenomenex Jupiter 3μ C18 (150x2.0 mm) column with a flow rate of 0.2 $mL \cdot min^{-1}$. Peptides were purified by RP-HPLC on AXIA Proteo 4u

90 Å250x21.2mm column. HPLC analyses and purification were performed using gradients of CH_3CN (0.1% TFA) (solvent A) in water (0.1% TFA) (solvent B)

iNGRt peptides:

- E5-Ahx-CRNGR

  Purification method: from 5 to 70% solvent A in B in 20 minutes

  MS Calculated mass (Da): 1360.46 found: 1360.74; $[M+H]^+$ = 1361.74; $[M+2H]^{2+}$= 681.43.

- K(Palm)-Ahx-CRNGR

  Purification method: from 30 to 85% solvent A in B in 20 minutes

  MS Calculated mass (Da): 1080.76 found: 1080.38; $[M+H]^+$ = 1081.38; $[M+2H]^{2+}$= 541.19.

iNGR peptides:

- E5-Ahx-iNGR(cyclic)

  Sequence: EEEEE-Ahx-CRNGRGPDC-NH_2 (cyclic)

  Purification method from 5 to 70% solvent A in B in 30 minutes

  MS Calculated mass (Da): 1733.86; found: 1733.74; $[M+2H]^{2+}$= 867.87

- K(Palm)-Ahx-iNGR (cyclic)

  Sequence: K(Palm)-Ahx-CRNGRGPDC-NH_2 (cyclic)

  Purification method: from 5 to 85% solvent A in B in 30 minutes

  MS. Calculated mass (Da): 1452.90; found: 1452.81; $[M+2H]^{2+}$= 727.9

NGR peptides:

- E5-Ahx- CNGRC- NH_2 (cyclic)

  Purification method: from 5 to 70% solvent A in B in 20 minutes

  Calculated mass (Da): 1306.46; found: 1306.59; $[M+H]^+$= 1307.59; $[M+2H]^{2+}$= 654.29.

- K(Palm)- Ahx- CNGRC- NH_2 (cyclic)

  Purification method: from 30 to 85% solvent A in B in 20 minutes

  MS Calculated mass (Da): 1027.50; found: 1028.68; $[M+2H]^{2+}$= 514.84.

2.3 Nanoparticle preparation

NPs were prepared by nanoprecipitation. Briefly, 5 mg of daPCL were dissolved in 1 mL of acetone and 2 mL of water were used as the aqueous phase. Peptides modified with PolyE or Palm (200 µg-500 µg corresponding to 4-10% theoretical loading) were added to the aqueous or organic phase, respectively. Once fully solubilized, the organic phase was added drop by drop to the aqueous phase under stirring at 400 rpm (revolutions per minute). After 30 min, the solution was then rotary evaporated (Rotavapor R-100) at 25 mBar and 80 rpm. The solution was then transferred to a 2 mL Eppendorf tube. For DiI-loaded NPs, 50 µg of DiI were added (by adding 50 µL of a 1 mg/mL DiI stock solution in DCM and allowing it to evaporate to form a film) into the organic phase before the beginning of the procedure as previously described. For DTX-loaded NPs, 250 µL of DTX in acetone (1 mg/ml stock) were added to polymer-containing acetone. In the experiments, stocks of PolyE in H_2O and Palm in MeOH were prepared at a concentration of 1 mg/mL or 2 mg/0.8 mL for formulations requiring 200 or 300-500 µg of the peptides.

2.4 Nanoparticle characterization

Hydrodynamic diameter (D_H), polydispersity index (PDI) and zeta potential (ξ) of NPs were determined on prepared NPs by a Zetasizer Nano Z (Malvern Instruments Ltd). Results are reported as mean DH of three separate measurements of three different batches (n = 9) ± standard deviation (SD). The yield of NP production process was evaluated on an aliquot of NP dispersion by weighting the solid residue after freeze-drying. Results are expressed as the ratio of the actual NP weight to the theoretical polymer weight × 100. The morphology of NPs was inspected by transmission electron microscopy (TEM) (CM 12 Philips, Eindhoven, The Netherlands) after staining with phosphotungstic acid diluted in water (1% w/v). The stability of NPs was evaluated in different media: 0.1 mL of NP dispersions were added to 0.9 mL of water, PBS (Phosphate buffer saline) at pH 7.4, DMEM

(Dulbecco's Modified Eagle Medium) with FBS (Fetal Bovine Serum) 10% and human plasma, incubated up to 72 h at 37 °C and measured size and zeta potential (ξ) values.

2.5 Peptide dosage and detachment

After preparation, NPs were purified through dialysis (0.4 mL of NP dispersion in a dialysis bag cut-off 3.5 kDa) against 3 mL of water. After 30 min, the samples inside the dialysis membranes and the external solution were freeze-dried (Telstar LyoQuest) for 24 h, reconstituted by adding 500 µL of DCM and 500 µL of water and centrifuged at 500 rpm for 15 min. The aqueous top layer (containing the peptides) was recovered and analyzed for peptide content by colorimetry through the Pierce Quantitative Assay. In particular, 180 µL of working reagent and 20 µL of samples were added to the required wells in a 96-well plate. The well plate was incubated for 30 seconds and then run in a spectrophotometer (Thermo Scientific TM Multiskan TM GO) at 480 nm. Absorbance was converted into concentration based on calibration curves for iNGR-PolyE or iNGR-Palm. The calibration curve for iNGR-PolyE and iNGR-Palm were generated by evaluating their absorbance in water and MeOH solutions, respectively, in the concentrations range 1-100 µg/mL.

The detachment of iNGR peptide from the NPs under physiologically-relevant conditions was assessed by placing a known amount of NPs in 10 mM phosphate-buffered saline at pH 7.4 (PBS) in a dialysis bag (cut-off 3.5 kDa). After different time points, the content of the membrane was collected and freeze-dried (Telstar LyoQuest). The samples were then reconstituted in 500 µL of DCM and 500 µL of H_2O, and centrifuged at 500 rpm for 15 min. The top layer was kept (for iNGR-Palm a further centrifugation step at 2000 rpm for 3 min was needed) and peptides were quantified by the colorimetric assay as previously described.

2.6 Preparation and characterization of DTX-loaded NPs

DTX loading inside NPs was assessed by placing 1 mg of freeze-dried NPs (without cryoprotectant) in 500 μL of acetonitrile, adding 500 μL of water, and filtering the samples through a 0.45 μm filter (Phenomenex, USA). DTX was analyzed by HPLC using a Shimadzu (Japan) apparatus equipped with an LC-10ADvp pump, a SIL-10ADvp autoinjector, an SPD-10Avp UV-Vis detector, and a C-R6 integrator. The analysis was performed on a Jupiter 5 μm, C18 column (250 x 4.6 mm, Å) (Phenomenex, USA). The mobile phase was a 55:45 (v/v) mixture of water with 0.1% TFA and acetonitrile pumped at a flow rate of 1 mL min^{-1}. The UV detector was set at 227 nm. A calibration curve for DTX in ethanol was plotted in the concentration range of 2–200 μg mL^{-1}. The release of DTX was determined on 0.5 mg NPs dispersed in 0.5 mL of 10 mM phosphate buffer containing NaCl (137 mM) and KCl (2.7 mM) at pH 7.4 (PBS) at 37°C placed in a dialysis bag (cut-off 3.5 kDa) using the same medium as the external phase (5 mL). At predetermined times, 1 mL aliquots of the sample were collected and then analyzed by HPLC to evaluate the actual loading of DTX in NPs, as previously reported. The results are expressed as % release ± SD of three experiments.

2.7 Cell studies

2.7.1 Cell cultures and treatments

Cell studies were carried out on MDA-MB231 and MRC-5 cell lines (ATCC) cultured in DMEM supplemented with 10% heat-inactivated FBS (Invitrogen, Life Technologies, Italy), 1.5 mM L-glutamine, 100 units/mL penicillin, and 100 μg/mL streptomycin under a humidified atmosphere of 5% CO_2 at 37°C.

2.7.2 MTT assay

MDA-MB231 and MRC-5 cells were seeded onto 96-well plates (1 x 10^4 cells/well) and incubated with NPs for 24 h and 72h. Then, cell viability was evaluated by the 3-(4,5-dimethylthiazol-2-yl)-2,5-diphenyl-2H-tetrazolium bromide (MTT) assay (Virgilio et al., 2020). The absorbance was

measured at 570 nm using a microplate reader (Biotek Synergy H1 Hybrid multiplate reader). In the case of unloaded NPs, the experiment was performed only on the MDA-MB231 cell line. Treatments were performed by replacing the culture medium with a dispersion of daPCL NPs, daPCL/iNGRt-PolyE or daPCL/iNGRt-Palm NPs in the same medium (0.001 – 0.5 mg/mL) and free peptides as a comparison (iNGR-PolyE and iNGR-Palm). In the case of DTX-loaded NPs, the experiment was performed on both cell lines treated with increasing concentrations of NPs ([DTX] in the range 0.001 – 0.1 μg/mL).

2.7.3 Cell uptake of NPs

The uptake of NPs in MDA-MB231 cells was evaluated on DiI-loaded NPs (0.05 mg/mL) by measuring the concentration of the fluorescent probe DiI. Briefly, cells (1.5×10^4 cells per well in 24-well plates) were collected and analysed by fluorimetry on a Cary Eclipse fluorescence spectrophotometer (Varian). A calibration curve of NPs in the medium was built in the concentration range 0.001-0.1 mg/mL. Excitation and emission wavelengths were 549 and 565 nm, respectively (Maiolino et al., 2015).

For fluorescence microscopy, MDA-MB231 cells were plated on coverslips at a density of 2×10^4 cells per well into 35 mm tissue culture plates, treated with DiI-labeled NPs (0.05 mg/mL) and observed 24 h later.

2.7.5 Confocal microscopy

MDA-MB231 cells were plated on coverslips at a density of 2×10^4 cells per well in 12-well plates as previously reported and incubated with DiI-loaded NPs (0.05 mg/mL). Images were acquired on a Zeiss LSM 510 meta confocal microscope equipped with an oil immersion plan Apochromat 100× objective 1.4 NA. The laser line was set at 549 nm for DiI and 405 nm for DAPI. Images were collected simultaneously in red and blue channels and as z-stack.

2.7.6 Western Blot analysis

Protein extracts were prepared as previously described (Pecoraro et al., 2020). Western blot analysis was performed as previously reported (De Filippis et al., 2008). The membranes were challenged with anti-Neuropilin-1 (Cell Signaling Technology, Danvers, MA, USA), and anti-α-tubulin (Santa Cruz, Dallas, TX, USA). Proteins were visualized with an enhanced chemiluminescence detection reagent according to the manufacturer's instructions (Elabscience®, Houston, TX, USA).

2.8 In vivo studies

The antitumor effects of NPs were tested in a heterotopic mouse model of triple-negative breast cancer. The experimental protocols performed in this study complied with the European Community Council directive (86/609/EEC). All the experiments on animal models complied with the guidelines for the Care and Use of Laboratory Animals of the National Cancer Institute – IRCCS – "Fondazione G. Pascale". Twenty-eight-week-old female Foxnnu/nu mice (Envigo, San Pietro al Natisone, Italy) were housed 5 per cage and maintained on a 12-h light:12-h dark cycle (lights on at 7.00 a.m.) in a temperature-controlled room (22±2°C) and with food and water ad libitum. All efforts to minimize animal suffering were made. After 1-week of acclimation to the housing conditions, mice were injected subcutaneously (s.c.) with a suspension of MDA-MB231 cells (5×10^6 cells/mouse in the right hind limb). After 1 week, when tumours reached 30–60 mm^3, mice were randomized based on tumour volume and weight according to Fisher's exact test into control and treatment groups (6 animals per group). Mice received one i.v. administration into the caudal vein of NaCl 0.9% (control), empty daPCL NPs, free DTX, DTX-daPCL NPs and DTX-daPCL/iNGRt-Palm NPs (in PBS) at a DTX dose of 5 mg/kg. After 6 days, mice received a second dose. Tumour growth was measured every 2–3 days with a digital calliper 2BIOL (Besozzo, Italy) and expressed as volume, according to the formula: $V = (a \times b^2)/2$ (a = the largest superficial diameter and b = the smallest superficial diameter). Animals were sacrificed with cervical dislocation when they reached the cut-off of 1500

mm^3 or when presenting signs of pain. Normally distributed data were represented as mean ± S.E.M. Two-way ANOVA and Tukey's test of post-hoc analysis were used to examine the significance of differences among groups (Graph pad Prism 5.0). A probability value with *P < 0.05 and **P < 0.01 *** P< 0.001 **** P<0.0001 was considered to be statistically significant.

RESULTS AND DISCUSSION

3.1 Synthesis of the peptides and preparation of peptide decorated NPs

The functionalization of NPs with the peptides was achieved by exploiting non-covalent interactions between daPCL and a modified variant of NGR peptides. The sequence CRNGR (iNGRt), containing the CendR motif, was derivatized with an aminohexanoic linker (Ahx) and then either the E5 sequence (polyE) or the palmitoyl chain (Palm). The peptide polyE-Ahx-CRNGR with an isoelectric point of 4.33 was designed to be adsorbed at a neutral pH on the surface of positively charged daPCL NPs. The peptide K(Palm)-Ahx-CRNGR, bearing a palmitoyl unit on the side chain of the N-terminal lysine was designed to interact by hydrophobic forces with the aliphatic chains of daPCL previously developed to fabricate amine-NPs (Fig. 1) (Conte et al., 2019a). NPs are expected to have a core-shell structure where the external peptide shell surrounds the hydrophobic core entrapping the lipophilic anticancer drug. To our knowledge, this is the first time that such a mode of functionalization of NP surface with targeting peptides is reported.

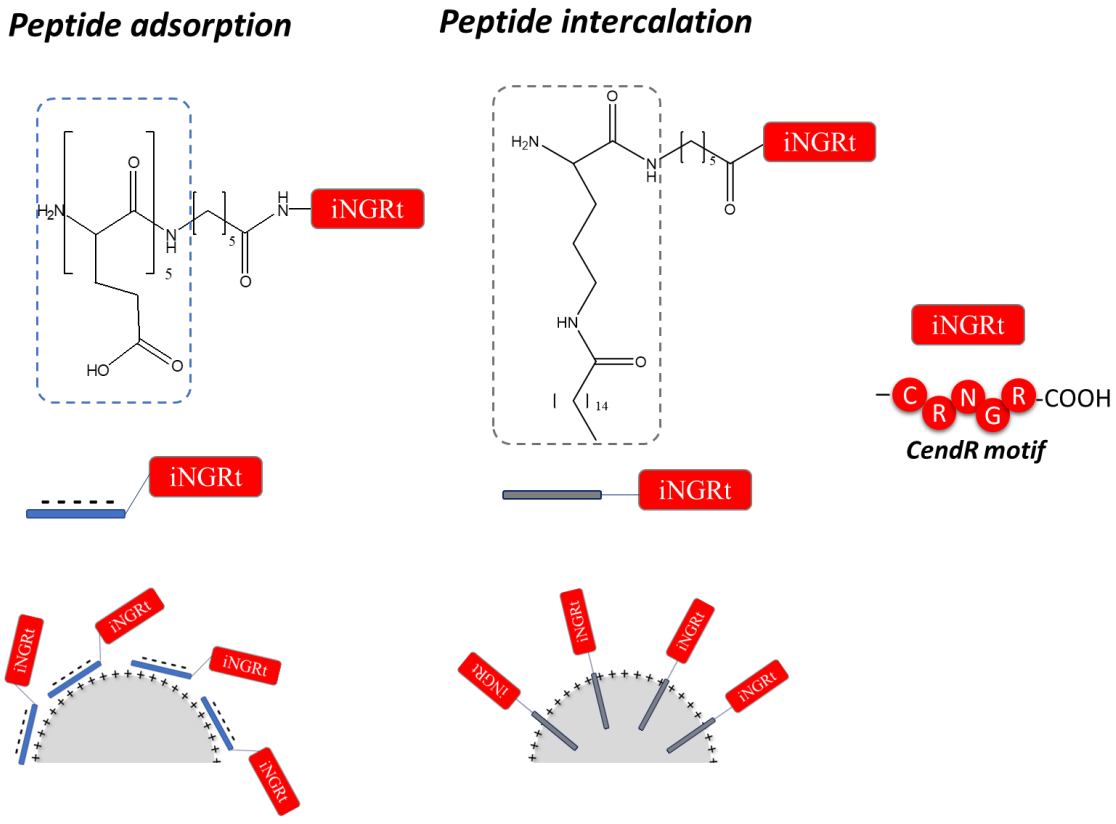

Figure 1. Sketched representation of peptides structures and of NP design.

To produce NPs via nanoprecipitation, iNGRt-PolyE was solubilized into the aqueous phase, whereas iNGRt-Palm was added to the polymer-containing organic phase. As a first step, we performed an in-depth formulation study to evaluate the amount of peptide anchored to NPs. We tested a peptide amount in the preparation of NPs ranging from 200 to 500 μg per 5 mg of daPCL (4-10% theoretical loading). As a control, we also prepared daPCL NPs (without peptides).

Table 1. Properties of peptide decorated NPs.

Batch	**D_H (nm ± SD) [a]**	**PDI [a]**	**ζ [a] (mV± SD)**	**Yield (%)**
daPCL NPs	105 ± 4	0.122 ± 0.015	+34 ± 7	92
daPCL/iNGR-PolyE NPs	110 ± 5	0.106 ± 0.026	+32 ± 5	87
daPCL/iNGRt-Palm NPs	102 ± 3	0.134 ± 0.012	+28 ± 2	85

[a] evaluated by PCS.

As evident in Table 1, independently by the presence of the peptides, all the formulations showed hydrodynamic diameters (D_H) ~100 nm, low polydispersity indexes and high yield of the formulation process. The yield of the preparation process, calculated weighting the solid residue after NP freeze-drying, was very high for all the formulations indicating that daPCL is suitable to generate NPs. The functionalization with the peptides, either intercalated or adsorbed, induced only a slight decrease of ζ, due to the peptide ability to partially shield NP cationic surface. The stability of peptides-functionalized NPs was evaluated in different biological fluids (cell medium enriched with proteins, PBS and human plasma) to anticipate their behaviour in biologically-relevant conditions. As shown in Fig. 2A, both NPs types were stable up to three days of incubation in all the media analyzed, with a reversal of ζ in plasma and cell medium due to protein adsorption. In Fig. 2B, the amount of peptides associated to NPs at different theoretical peptide levels (from 4 to 10 % w/w) are reported. We found that, independently by the theoretical loading and modification strategy, a maximum amount of ca.

150 μg of peptides was effectively associated to NPs, thus suggesting that the surface area of NPs is critical to attain surface-modification.

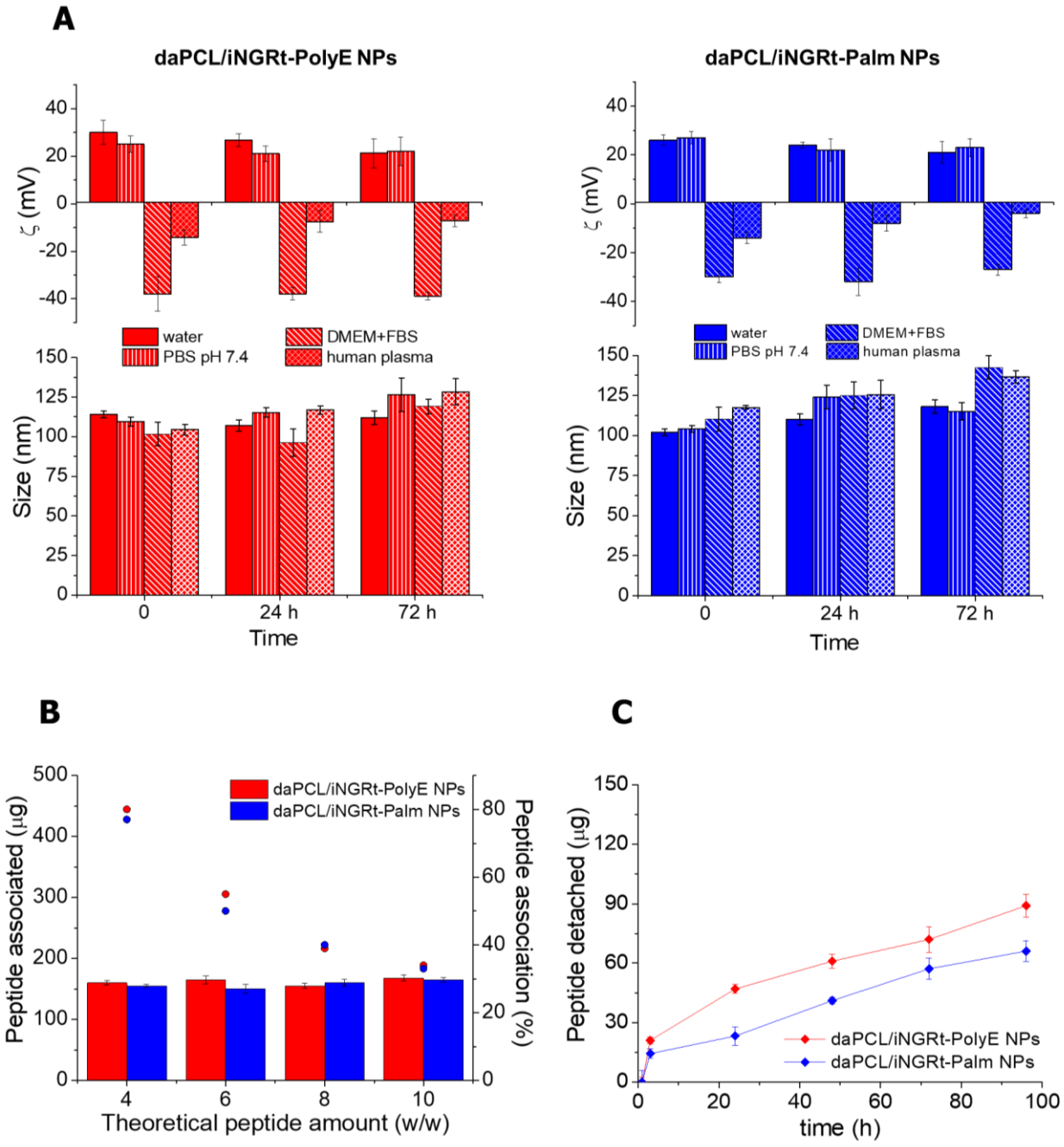

Figure 2. A) Stability of daPCL/iNGRt-Palm NPs and daPCL/iNGRt-PolyE NPs in different simulated biological media up to 72 h of incubation at 37°C; B) Amount of iNGRt associated with NPs (2.5 mg/mL); C) *In vitro* detachment of iNGRt from daPCL NPs in PBS 10 mM at pH 7.4 and 37 °C. Results are expressed as μg of peptide detached over time ± SD of three experiments.

Finally, the detachment of both peptides from NPs prepared at 4% theoretical peptide loading was investigated at 37°C and pH 7.4 (Fig. 2C). Independently of the integration method, an initial detachment (15% of peptides in the first 6 h of incubation) was observed. While the detachment of iNGR-PolyE was expected due to the labile nature of electrostatic interactions, the burst of iNGR-Palm can be explained by assuming that iNGRt migrates to the NP surface despite it was added in the polymer phase during nanoprecipitation. In the second release stage, peptides were detached at a slower rate in the case of iNGRt Palm as compared to iNGRt-PolyE, thus confirming a different mode of interaction with the NP surface.

3.2 Biological performance of peptide-functionalized NPs

The cytotoxicity of untargeted (daPCL NPs) and targeted NPs (daPCL/iNGRt-PolyE and daPCL/iNGRt-Palm) was evaluated in 2D MDA-MB231 cancer cells, a triple-negative breast cancer cell line, after assessing the overexpression of NRP-1 (Fig. S1). Cells were incubated with a wide range of NP concentrations (from 0.001 to 0.5 mg/mL) and tested upon 24 h and 72 h of treatment. As evident from the results reported in figure 3A and figure S2, daPCL NPs showed a time- and dose-dependent cytotoxicity, probably due to the well-known toxicity of cationic polymers (Lv et al., 2006). However, a slightly different behaviour was observed in the presence of the two different peptides, especially at 72 h (Fig. S2A). In particular, the adsorption of iNGRt-PolyE seems to alleviate the cytotoxicity of unloaded daPCL NPs, whereas the integration with iNGRt-Palm slightly increases their intrinsic toxicity. No toxicity of free iNGRt-PolyE or iNGRt-Palm was found at 24 h whereas a slight decrease of cell viability was observed at 72 h, especially with free iNGRt-Palm at the highest concentration tested (Fig. S2C). This effect could be related to the recent evidence of antiproliferative activity of palmitic acid on different cancer cell lines, the underlying mechanisms being still unexplored (Baumann et al., 2016; Fite et al., 2007; Jozwiak et al., 2020; Murray et al., 2015).

Next, all the formulations were loaded with a fluorescent lipophilic dye (DiI) (colloidal properties are reported in Table S1) and their intracellular uptake was studied in MDA-MB231 cells. As a control for the uptake experiment, we produced peptides with the E5-Ahx or K(Palm)Ahx linkers connected to the cyclic peptides iNGR (CRNGRGPDC) and NGR (CNGRC), which are not recognized by NRP-1. In fact, iNGR contains a cryptic CendR sequence that is exposed only after its interaction with the CD13 receptor on endothelial cells whereas the NGR peptide recognizes the CD13 receptor (which is not expressed in cancer cells) (Soudy et al., 2012). The activation of the CendR sequence by proteolytic cut and ring-opening occurs only upon recognition of iNGR by CD13 on the surface of tumor endothelial cells. On the contrary NGR does not cointain a CendR motif. Both iNGR as such and NGR are expected not to mediate delivery of NP to cells overexpressing NRP-1, such as MDA-MB231. Cells were incubated with DiI-NPs (0.05 mg/mL) for 6 h and 24 h. The fluorescence intensity of the internalized DiI-NPs was measured by fluorimetry. As shown in Fig. 3B, the treatment with daPCL/iNGRt-PolyE NPs as well as daPCL/iNGRt-Palm NPs was associated with an increasing time-dependent cellular uptake (30% and 70-80% after 6 h and 24 h, respectively). The presence of iNGR and NGR peptides did not provoke any significant increase in NPs uptake, confirming that NPs internalization was driven by their binding with NRP-1 receptor (Alberici et al., 2013; Liu et al., 2011). Notably, no difference in NP uptake between daPCL/iNGRt-PolyE NPs and daPCL/iNGRt-Palm NPs was observed after 24 h of incubation, thus demonstrating the efficacy of both functionalization strategies to promote the entry of NPs into cancer cells. The accumulation of iNGRt-modified NPs into MDA-MB231 cells was confirmed by fluorescence microscopy (Fig. 3C and Fig. S3).

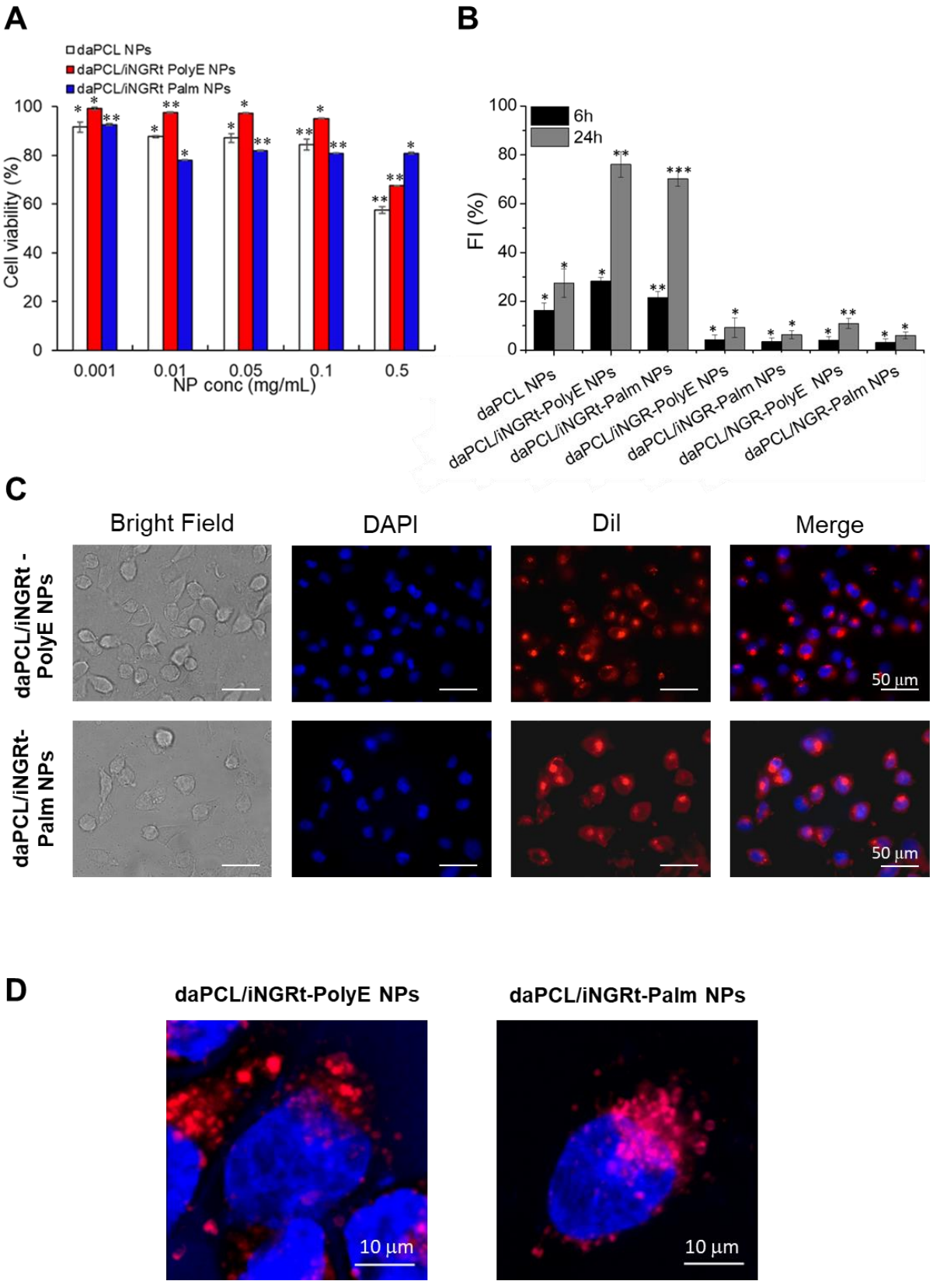

Figure 3. A) Cytotoxicity of daPCL NPs, daPCL/iNGRt-PolyE NPs, daPCL/iNGRt-Palm NPs in MDA-MB231 cells after 24 h of treatment. * $p < 0.05$; ** $p < 0.01$. B-D) Internalization of DiI-labeled NPs in MDA-MB231 cells: (B) Amount of NPs inside cells after 6 and 24 h. iNGR and NGR are not recognized by NRP-1 receptor and used as control. Bars represent mean values ± SEM of

three experiments. (C) Phase contrast and Fluorescence microscopy images of MDA-MB231 cells after incubation with DiI-labeled NPs (red) for 24 h. (D) Confocal microscopy images of MDA-MB231 cells after 24 h of incubation with DiI-labeled NPs (red) (0.05 mg/mL). Cell nuclei stained with DAPI (blu).

Next, to investigate the subcellular distribution of internalized NPs, we carried out confocal laser scanner microscopy (CLSM) analysis of MDA-MB231 cells after 24 h of incubation with fluorescent and nuclear staining with DAPI (Fig 3D). As shown in Fig. 3D, a different intracellular localization of the formulations was observed since daPCL/iNGRt-Palm NPs were mainly located at the perinuclear level whereas daPCL/iNGRt-PolyE NPs were mainly distributed into the cytosol.

3.3 Preparation of DTX loaded NPs

In a second step, Docetaxel (DTX), a taxane with well-known antimitotic activity, was selected as active cargo to establish a proof of concept of functional delivery. After a preliminary formulation study (Table S2), DTX was loaded into NPs at 5% w/w. Colloidal properties of DTX formulations, with or without CendR peptides are reported in Table 2.

Table 2. Colloidal properties of DTX-loaded NPs.

Formulation	**Size (nm ± SD)**	**ζ (mV± SD)**	**P.I.**	**Yield (%)**	**Actual loading DTX (mg /100 mg NPs)**	**Entrapment efficiency (%)**
DTX-daPCL NPs	120 ± 2	+32 ± 7	0.1	85	4.7	98±3
DTX-daPCL/iNGRt-PolyE NPs	95 ± 4	+30 ± 5	0.1	80	4.17	95±7
DTX-daPCL/iNGRt-Palm NPs	96 ± 8	+33 ± 2	0.2	85	4.26	96±3

The loading of DTX at 5% w/w was complete and did not alter the overall colloidal properties of the nanoplatform. TEM images of peptide-coated NPs were spherical as shown in Fig. 4A. Size distribution curves of NPs dispersed in different media showed high stability in the tested media, similarly to the unloaded ones (Fig. 4C). Release profiles of DTX from the nanoplatform were investigated at 37 °C and pH 7.4. Independently of the peptide added into NPs, DTX was released in

a sustained manner (Fig. 4B). In fact, after an initial burst effect (15% of DTX in the first 6 h of incubation), 50% of the drug entrapped was released in around 48 h, thus highlighting the ability of NPs to sustain the release of the anticancer drug. The slower burst observed for iNGRt-Palm NPs can be explained by the presence of long alkyl chains of the peptide that alter DTX rearrangement in the NP core.

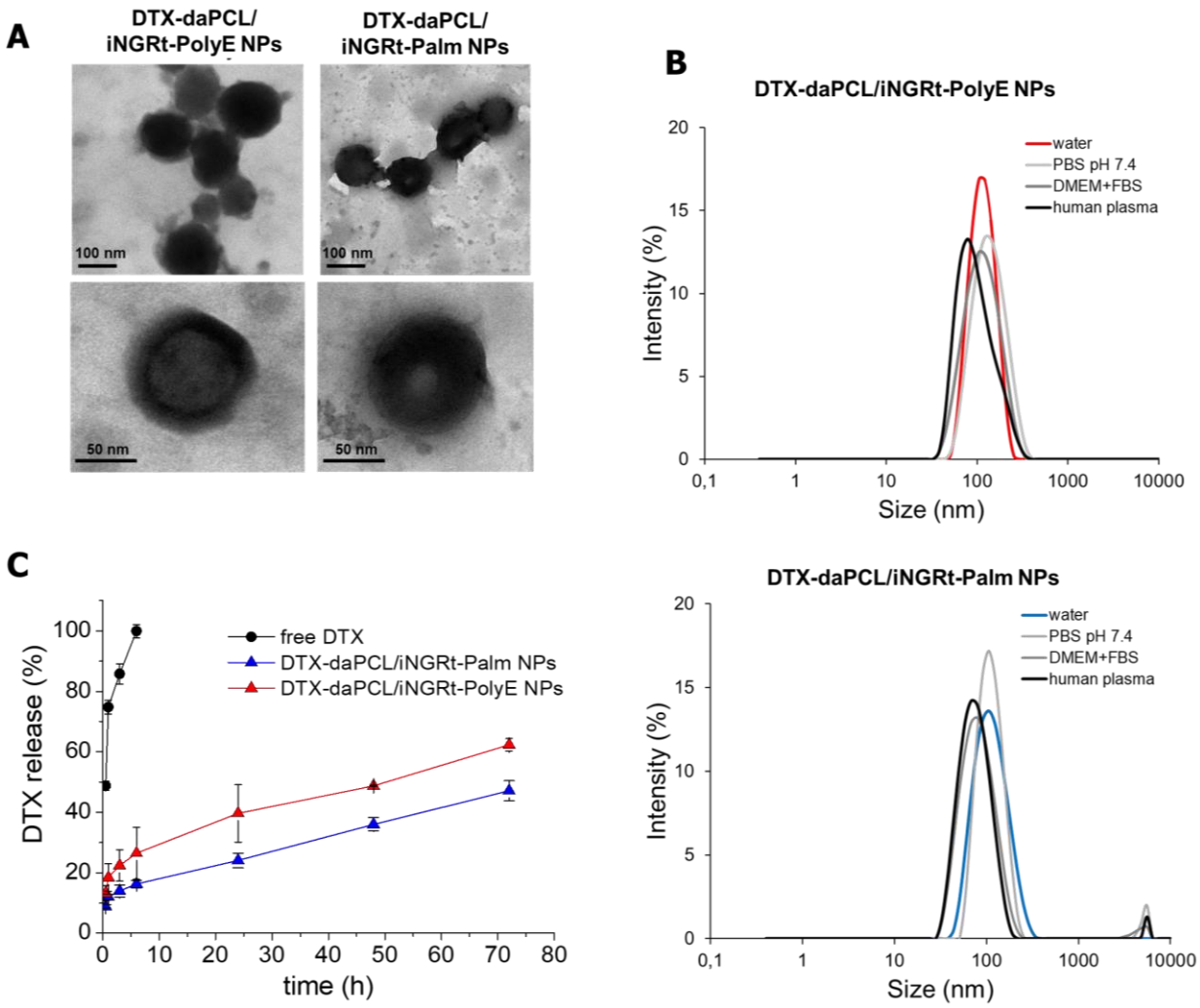

Figure 4. A) TEM images of DTX-loaded NPs decorated with iNGRt-Palm or iNGRt-PolyE; B) Stability of DTX-NPs decorated with peptides in different simulated biological media after 72 h of incubation. C) *In vitro* release of DTX from daPCL NPs decorated with iNGRt-Palm or iNGRt-PolyE in PBS 10 mM at pH 7.4 and 37 °C. Results are expressed as release % over time ± SD of three experiments.

The cytotoxicity of DTX-loaded NPs was assessed on MDA-MB231 and MRC-5 fibroblasts, where the expression levels of the NRP-1 receptor are very low (Fig. S1). In vitro cytotoxicity of DTX-

loaded NPs was evaluated after 24 and 72 h with DTX-loaded NPs at different DTX concentrations (0.001-0.1 μg/mL) by using the MTT assay. Results shown in Fig. 5 demonstrated a time- and dose-dependent cytotoxicity of free DTX in both cell lines with a similar trend. In the case of MDA-MB231 cells, a time- and dose-dependent cytotoxicity of the formulations was evidenced. However, at both time points, peptide-functionalized DTX-daPCL NPs showed higher cytotoxicity as compared to untargeted DTX-daPCL NPs, especially in the case of DTX-daPCL/iNGRt-Palm NPs that reduced cell viability at 90% after 72 h at 0.1 μg/mL of drug dose (daPCL/iNGRt-Palm NPs *vs* daPCL/iNGRt-PolyE NPs $p < 0.001$). Based on the extent of internalization observed, it is expected that iNGRt-bearing NPs show higher cytotoxicity compared with untargeted NPs. The remarkable effect of palmitoylated NPs could be related to the presence of the palmitoyl chain in the peptide that can increase DTX activity. Several studies have demonstrated an increase in DTX activity in the presence of fatty acids, including palmitic acid due to different mechanisms (Fite et al., 2007; Goupille et al., 2020; Shaikh et al., 2008). Furthermore, the perinuclear localization of daPCL/iNGRt-Palm NPs can increase DTX activity due to the reorganization of the microfilament network which results in novel ring-like formations of F-actin condensed exclusively in this region, as previously reported (Rosenblum and Shivers, 2000).

DTX-loaded NPs were more cytotoxic against MDA-MB231 cells, compared to MRC-5 cells, thus demonstrating that NP cell uptake is effectively driven to breast cancer cells due to overexpression of the NRP-1 receptor (Fig S1). In particular, all the DTX-loaded formulations, reduced the cell viability of MRC-5 cells of only 20% at the highest dose tested with dose- and time-dependent comparable patterns while DTX alone killed the 80% of cells at the same time (Fig. 5). On the whole, cytotoxicity data indicate that NPs maintain the efficacy of DTX on cancer cells alleviating its toxicity toward normal fibroblasts.

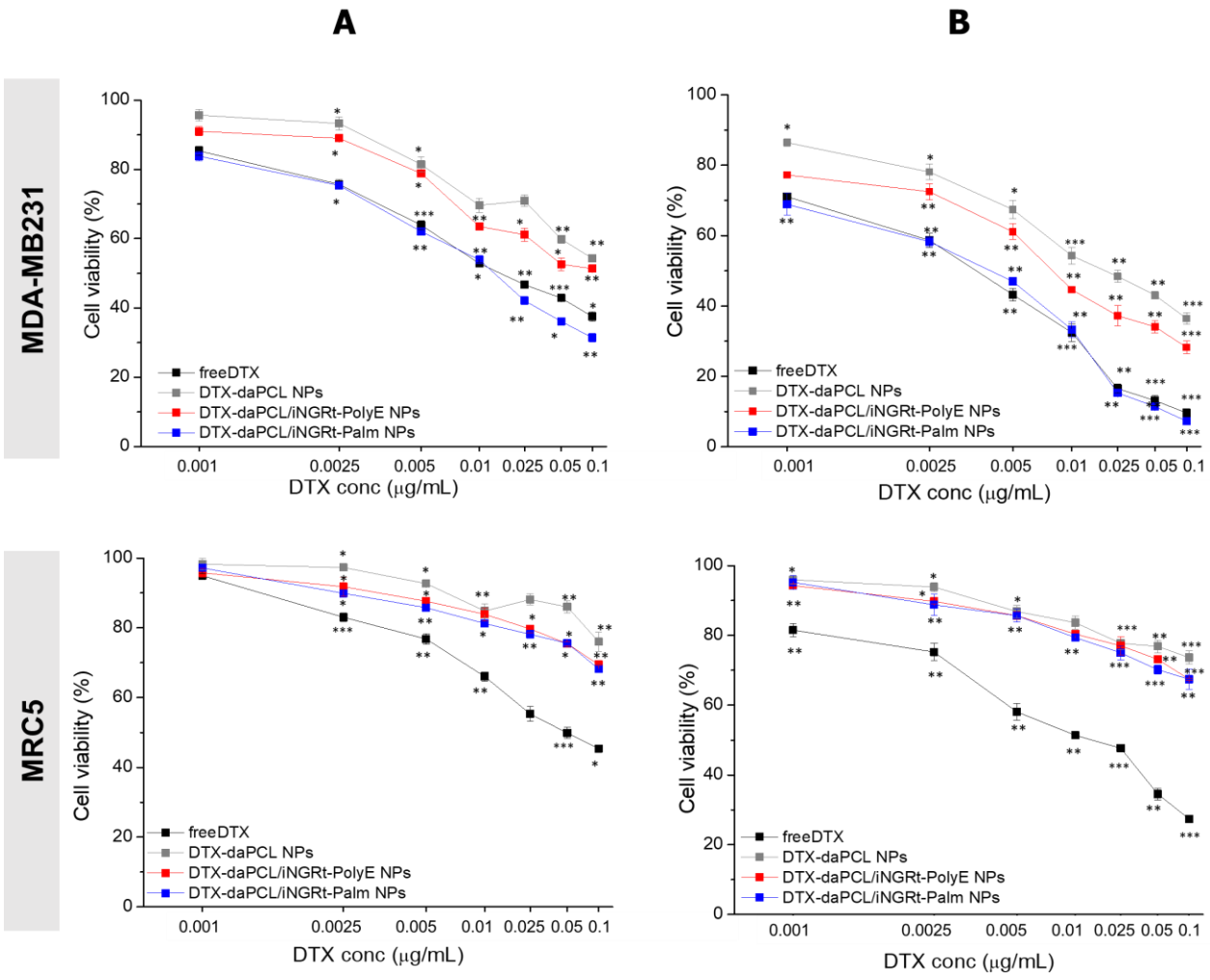

Figure 5. Cytotoxicity of DTX loaded-NPs in MDA-MB231 and MRC-5 fibroblasts after 24 h (A) and 72 h (B). After incubation, cell viability was evaluated using the MTS assay. The cell viability from untreated cells was set to 100%. Data represent the average of three independent experiments; error bars represent the standard deviation. *$p < 0.05$; **$p < 0.01$; ***$p < 0.001$ vs. untreated.

3.4 In vivo antitumoral activity of NPs

Due to the promising cytotoxicity and selectivity of DTX-daPCL/iNGRt-Palm NPs, we moved to in vivo studies in a heterotopic mouse model of triple-negative breast cancer. Mice received different treatment by i.v. injection when the tumours were palpable and reached a dimension of 100 mm^3 and subdivided into the following groups: saline (CTRL), free DTX, daPCL NPs, DTX-daPCL NPs and DTX-daPCL/iNGRt-Palm NPs, at a DTX dose of 5 mg/kg. No body weight variations in mice treated with DTX-loaded NPs were observed whereas DTX significantly decreased animal weight as compared to control (Fig. 6A). As shown in Figure 6B, five days post first injection, the animals

treated with DTX showed a not significant drop-down of tumour weight and growth compared with the control group ($p > 0.05$). Free DTX started to inhibit the tumour growth after the second administration performed 7 days after the first injection, whereas DTX-daPCL/iNGRt-Palm exerted a remarkable anticancer after the first injection ($P<0.05$). At the end of the experiment, DTX-daPCL/iNGRt-Palm NPs resulted to be more effective than DTX-daPCL NPs in reducing the tumor volume. The survival of animals closely followed the tumour growth profile. Kaplan–Meier results (Fig. 6C) showed an increased median of survival for DTX-daPCL NPs and DTX-daPCL/iNGRt-Palm NPs treated mice compared with the control groups (CTRL and empty NPs, $P = 0.001$ determined using log-rank test) as well as the group treated with free DTX at 34 days.

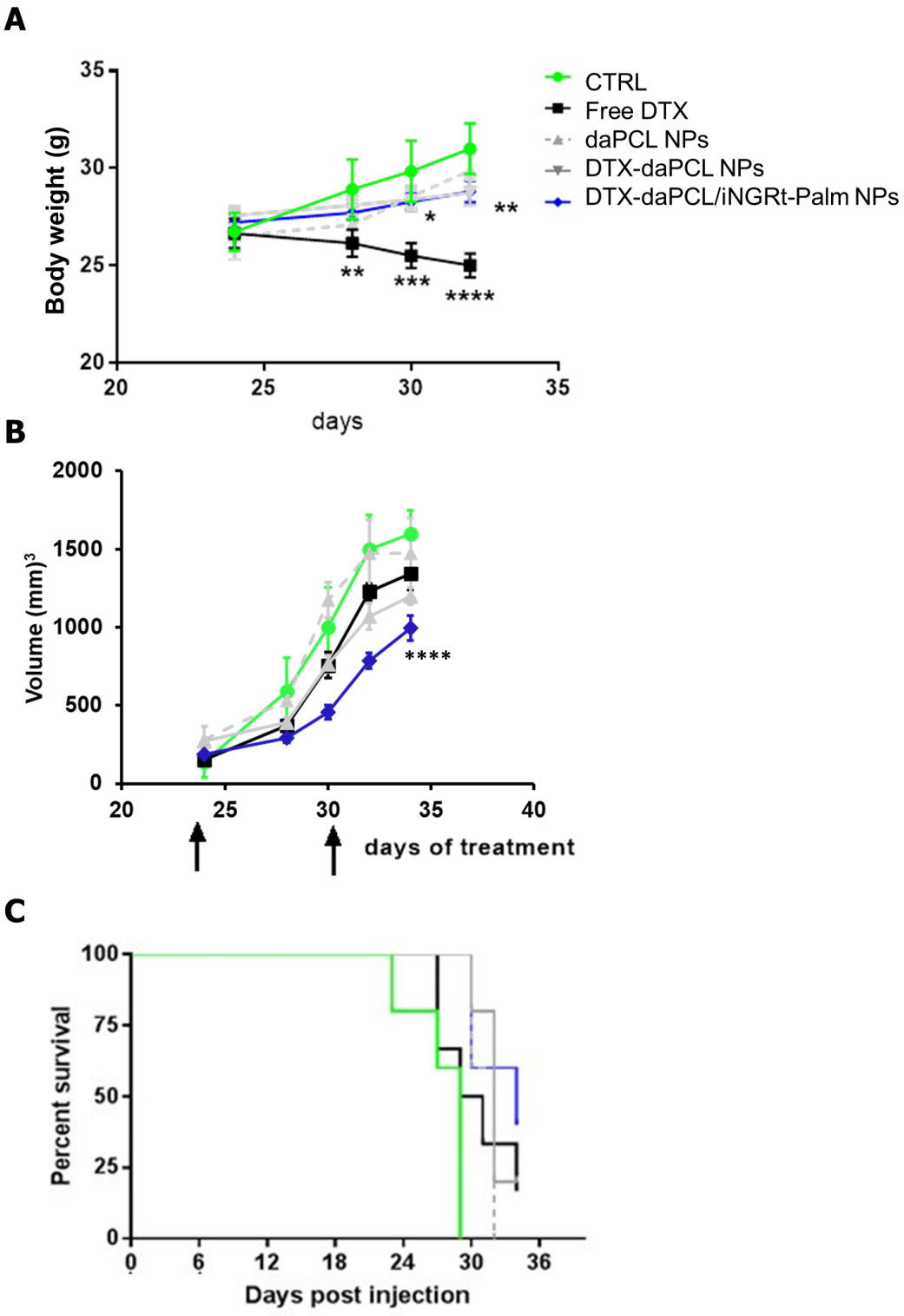

Figure 6. Body weight (A), tumor growth inhibition (B) and Kaplan–Meier survival plot (C) of female athymic Fox nu/nu mice nude mice bearing subcutaneous MDA-MB231 tumor. Mice received at T0 and after 6 days of treatment an i.v. injection of saline (CTRL), empty NPs (daPCL NPs), free DTX and DTX-loaded NPs without or with the peptide (DTX-daPCL NPs and DTX-daPCL/iNGRt-Palm NPs). DTX dose was 5 mg/kg. **p< 0.01 DTX-daPCL NPs vs saline; ****p < 0.0001 DTX-daPCL/iNGRt-Palm NPs vs saline.

CONCLUSIONS

We have developed biodegradable NPs based on a diamino-terminated poly(ε-caprolactone) decorated on the surface with NGR peptides, to allow the active targeting versus neuropilin receptors (NRP), overexpressed on tumour endothelia and cancer cells. We have demonstrated that the targeting peptide can be anchored on the NP surface through two different non-covalent binding approaches, thus modulating NP formulation, due to the versatility of the nanoplatform features. NPs showed high efficiency in exposing the peptide on the surface, useful for the selective interaction and consequently high cell internalization in breast cancer cells. Furthermore, the encapsulation of Docetaxel (DTX) as a lipophilic anticancer drug into the NP core conferred anticancer potential to the system, as demonstrated in both *in vitro* and *in vivo* models of triple-negative breast cancer.

ASSOCIATED CONTENT

Supporting Information. A PDF file is supplied as Supporting Information.

Properties of DiI loaded NPs, formulation studies of DTX entrapment, Neuropilin expression in MDA-MB231 cells and MRC-5 fibroblasts, cytotoxicity of peptide decorated NPs and free peptides in MDA-MB231, internalization of DiI-loaded NPs in MDA-MB231 cells after 6 h.

AUTHOR INFORMATION

Corresponding Author

Email: **claudia.conte@unina.it**

Notes The authors declare no competing financial interest.

Author Contributions

The manuscript was written through contributions of all authors. All authors have given approval to the final version of the manuscript.

ACKNOWLEDGMENT

This work was supported by Italian Association for Cancer Research (IG2014 #15764).

REFERENCES

Alberici, L., Roth, L., Sugahara, K.N., Agemy, L., Kotamraju, V.R., Teesalu, T., Bordignon, C., Traversari, C., Rizzardi, G.P., Ruoslahti, E., 2013. De novo design of a tumor-penetrating peptide. Cancer Res 73, 804-812.

Aubin-Tam, M.E., Hamad-Schifferli, K., 2008. Structure and function of nanoparticle-protein conjugates. Biomed Mater 3, 034001.

Baumann, J., Wong, J., Sun, Y., Conklin, D.S., 2016. Palmitate-induced ER stress increases trastuzumab sensitivity in HER2/neu-positive breast cancer cells. BMC Cancer 16, 551.

Bezzerri, V., Avitabile, C., Dechecchi, M.C., Lampronti, I., Borgatti, M., Montagner, G., Cabrini, G., Gambari, R., Romanelli, A., 2014. Antibacterial and anti-inflammatory activity of a temporin B peptide analogue on an in vitro model of cystic fibrosis. J Pept Sci 20, 822-830.

Brossard, C., Vlach, M., Vene, E., Ribault, C., Dorcet, V., Noiret, N., Loyer, P., Lepareur, N., Cammas-Marion, S., 2021. Synthesis of Poly(Malic Acid) Derivatives End-Functionalized with Peptides and Preparation of Biocompatible Nanoparticles to Target Hepatoma Cells. Nanomaterials (Basel) 11.

Cai, H., Liang, Z., Huang, W., Wen, L., Chen, G., 2017. Engineering PLGA nano-based systems through understanding the influence of nanoparticle properties and cell-penetrating peptides for cochlear drug delivery. Int J Pharmaceut 532, 55-65.

Conte, C., Dal Poggetto, G., B, J.S., Esposito, D., Ungaro, F., Laurienzo, P., Boraschi, D., Quaglia, F., 2019a. Surface Exposure of PEG and Amines on Biodegradable Nanoparticles as a Strategy to Tune Their Interaction with Protein-Rich Biological Media. Nanomaterials (Basel) 9.

Conte, C., Moret, F., Esposito, D., Dal Poggetto, G., Avitabile, C., Ungaro, F., Romanelli, A., Laurienzo, P., Reddi, E., Quaglia, F., 2019b. Biodegradable nanoparticles exposing a short anti-FLT1

peptide as antiangiogenic platform to complement docetaxel anticancer activity. Mater. Sci. Eng. C 102, 876-886.

De Filippis, D., Russo, A., D'Amico, A., Esposito, G., Pietropaolo, C., Cinelli, M., Russo, G., Iuvone, T., 2008. Cannabinoids reduce granuloma-associated angiogenesis in rats by controlling transcription and expression of mast cell protease-5. Br J Pharmacol 154, 1672-1679.

Delehanty, J.B., Boeneman, K., Bradburne, C.E., Robertson, K., Bongard, J.E., Medintz, I.L., 2010. Peptides for specific intracellular delivery and targeting of nanoparticles: implications for developing nanoparticle-mediated drug delivery. Ther Deliv 1, 411-433.

Esfandyari-Manesh, M., Abdi, M., Talasaz, A.H., Ebrahimi, S.M., Atyabi, F., Dinarvand, R., 2020. S2P peptide-conjugated PLGA-Maleimide-PEG nanoparticles containing Imatinib for targeting drug delivery to atherosclerotic plaques. DARU Journal of Pharmaceutical Sciences 28, 131-138.

Esposito, D., Conte, C., Dal Poggetto, G., Russo, A., Barbieri, A., Ungaro, F., Arra, C., Russo, G., Laurienzo, P., Quaglia, F., 2018. Biodegradable nanoparticles bearing amine groups as a strategy to alter surface features, biological identity and accumulation in a lung metastasis model. J. Mater. Chem. B 6, 5922-5930.

Fan, S., Zheng, Y., Liu, X., Fang, W., Chen, X., Liao, W., Jing, X., Lei, M., Tao, E., Ma, Q., Zhang, X., Guo, R., Liu, J., 2018. Curcumin-loaded PLGA-PEG nanoparticles conjugated with B6 peptide for potential use in Alzheimer's disease. Drug Delivery 25, 1091-1102.

Fite, A., Goua, M., Wahle, K.W., Schofield, A.C., Hutcheon, A.W., Heys, S.D., 2007. Potentiation of the anti-tumour effect of docetaxel by conjugated linoleic acids (CLAs) in breast cancer cells in vitro. Prostaglandins Leukot Essent Fatty Acids 77, 87-96.

Fosgerau, K., Hoffmann, T., 2015. Peptide therapeutics: current status and future directions. Drug Discov Today 20, 122-128.

Galindo, R., Sánchez-López, E., Gómara, M.J., Espina, M., Ettcheto, M., Cano, A., Haro, I., Camins, A., García, M.L., 2022. Development of Peptide Targeted PLGA-PEGylated Nanoparticles Loading Licochalcone-A for Ocular Inflammation, Pharmaceutics.

Gessner, I., Neundorf, I., 2020a. Nanoparticles Modified with Cell-Penetrating Peptides: Conjugation Mechanisms, Physicochemical Properties, and Application in Cancer Diagnosis and Therapy, International Journal of Molecular Sciences.

Gessner, I., Neundorf, I., 2020b. Nanoparticles Modified with Cell-Penetrating Peptides: Conjugation Mechanisms, Physicochemical Properties, and Application in Cancer Diagnosis and Therapy. Int J Mol Sci 21.

Goupille, C., Vibet, S., Frank, P.G., Maheo, K., 2020. EPA and DHA Fatty Acids Induce a Remodeling of Tumor Vasculature and Potentiate Docetaxel Activity. Int J Mol Sci 21.

Hoyos-Ceballos, G.P., Ruozi, B., Ottonelli, I., Da Ros, F., Vandelli, M.A., Forni, F., Daini, E., Vilella, A., Zoli, M., Tosi, G., Duskey, J.T., López-Osorio, B.L., 2020. PLGA-PEG-ANG-2 Nanoparticles for Blood–Brain Barrier Crossing: Proof-of-Concept Study, Pharmaceutics.

Jensen, L.D., Nakamura, M., Brautigam, L., Li, X., Liu, Y., Samani, N.J., Cao, Y., 2015. VEGF-B-Neuropilin-1 signaling is spatiotemporally indispensable for vascular and neuronal development in zebrafish. Proc Natl Acad Sci U S A 112, E5944-5953.

Jozwiak, M., Filipowska, A., Fiorino, F., Struga, M., 2020. Anticancer activities of fatty acids and their heterocyclic derivatives. Eur J Pharmacol 871, 172937.

Kadonosono, T., Yamano, A., Goto, T., Tsubaki, T., Niibori, M., Kuchimaru, T., Kizaka-Kondoh, S., 2015. Cell penetrating peptides improve tumor delivery of cargos through neuropilin-1-dependent extravasation. J Control Release 201, 14-21.

Kang, T., Gao, X.L., Hu, Q.Y., Jiang, D., Feng, X.Y., Zhang, X., Song, Q.X., Yao, L., Huang, M., Jiang, X.G., Pang, Z.Q., Chen, H.Z., Chen, J., 2014. iNGR-modified PEG-PLGA nanoparticles that recognize tumor vasculature and penetrate gliomas. Biomaterials 35, 4319-4332.

Li, J., Feng, L., Fan, L., Zha, Y., Guo, L., Zhang, Q., Chen, J., Pang, Z., Wang, Y., Jiang, X., Yang, V.C., Wen, L., 2011. Targeting the brain with PEG–PLGA nanoparticles modified with phage-displayed peptides. Biomaterials 32, 4943-4950.

Liu, C., Yu, W., Chen, Z., Zhang, J., Zhang, N., 2011. Enhanced gene transfection efficiency in CD13-positive vascular endothelial cells with targeted poly(lactic acid)-poly(ethylene glycol) nanoparticles through caveolae-mediated endocytosis. J Control Release 151, 162-175.

Lv, H., Zhang, S., Wang, B., Cui, S., Yan, J., 2006. Toxicity of cationic lipids and cationic polymers in gene delivery. J Control Release 114, 100-109.

Maiolino, S., Russo, A., Pagliara, V., Conte, C., Ungaro, F., Russo, G., Quaglia, F., 2015. Biodegradable nanoparticles sequentially decorated with Polyethyleneimine and Hyaluronan for the targeted delivery of docetaxel to airway cancer cells. J Nanobiotechnology 13, 29.

Murray, M., Hraiki, A., Bebawy, M., Pazderka, C., Rawling, T., 2015. Anti-tumor activities of lipids and lipid analogues and their development as potential anticancer drugs. Pharmacol Ther 150, 109-128.

Niza, E., Ocaña, A., Castro-Osma, J.A., Bravo, I., Alonso-Moreno, C., 2021. Polyester Polymeric Nanoparticles as Platforms in the Development of Novel Nanomedicines for Cancer Treatment, Cancers.

Paulino da Silva Filho, O., Ali, M., Nabbefeld, R., Primavessy, D., Bovee-Geurts, P.H., Grimm, S., Kirchner, A., Wiesmüller, K.-H., Schneider, M., Walboomers, X.F., Brock, R., 2021. A comparison of acyl-moieties for noncovalent functionalization of PLGA and PEG-PLGA nanoparticles with a cell-penetrating peptide. RSC Advances 11, 36116-36124.

Pearce, A.K., O'Reilly, R.K., 2019. Insights into Active Targeting of Nanoparticles in Drug Delivery: Advances in Clinical Studies and Design Considerations for Cancer Nanomedicine. Bioconjugate Chemistry 30, 2300-2311.

Pecoraro, A., Virgilio, A., Esposito, V., Galeone, A., Russo, G., Russo, A., 2020. uL3 Mediated Nucleolar Stress Pathway as a New Mechanism of Action of Antiproliferative G-quadruplex TBA Derivatives in Colon Cancer Cells. Biomolecules 10.

Rosenblum, M.D., Shivers, R.R., 2000. 'Rings' of F-actin form around the nucleus in cultured human MCF7 adenocarcinoma cells upon exposure to both taxol and taxotere. Comp Biochem Physiol C Toxicol Pharmacol 125, 121-131.

Ruoslahti, E., 2017. Tumor penetrating peptides for improved drug delivery. Adv Drug Deliv Rev 110-111, 3-12.

Seyyednia, E., Oroojalian, F., Baradaran, B., Mojarrad, J.S., Mokhtarzadeh, A., Valizadeh, H., 2021. Nanoparticles modified with vasculature-homing peptides for targeted cancer therapy and angiogenesis imaging. J Control Release 338, 367-393.

Shaikh, I.A., Brown, I., Schofield, A.C., Wahle, K.W., Heys, S.D., 2008. Docosahexaenoic acid enhances the efficacy of docetaxel in prostate cancer cells by modulation of apoptosis: the role of genes associated with the NF-kappaB pathway. Prostate 68, 1635-1646.

Shi, J., Kantoff, P.W., Wooster, R., Farokhzad, O.C., 2017. Cancer nanomedicine: progress, challenges and opportunities. Nat Rev Cancer 17, 20-37.

Soudy, R., Ahmed, S., Kaur, K., 2012. NGR peptide ligands for targeting CD13/APN identified through peptide array screening resemble fibronectin sequences. ACS Comb Sci 14, 590-599.

Sun, H., Dong, Y., Feijen, J., Zhong, Z., 2018. Peptide-decorated polymeric nanomedicines for precision cancer therapy. J Control Release 290, 11-27.

Teesalu, T., Sugahara, K.N., Kotamraju, V.R., Ruoslahti, E., 2009. C-end rule peptides mediate neuropilin-1-dependent cell, vascular, and tissue penetration. Proc Natl Acad Sci U S A 106, 16157-16162.

Virgilio, A., Esposito, V., Pecoraro, A., Russo, A., Vellecco, V., Pepe, A., Bucci, M., Russo, G., Galeone, A., 2020. Structural properties and anticoagulant/cytotoxic activities of heterochiral enantiomeric thrombin binding aptamer (TBA) derivatives. Nucleic Acids Res 48, 12556-12565.